surfaces

MDPI

Article

Ultra-Sensitive Immuno-Sensing Platform Based on Gold-Coated Interdigitated Electrodes for the Detection of Parathion

Shalini Nagabooshanam [1], Souradeep Roy [2], Shikha Wadhwa [3], Ashish Mathur [2,*], Satheesh Krishnamurthy [4] and Lalit Mohan Bharadwaj [5]

[1] Department of Chemical Engineering, SRM Institute of Science and Technology, Kattankulathur 603203, Tamil Nadu, India; shalini.bme@gmail.com
[2] Centre for Interdisciplinary Research and Innovation (CIDRI), University of Petroleum and Energy Studies, Dehradun 248007, Uttarakhand, India; souradeep.roy@ddn.upes.ac.in
[3] Department of Chemistry, University of Petroleum and Energy Studies, Dehradun 248007, Uttarakhand, India; shikha.wadhwa@ddn.upes.ac.in
[4] Nanoscale Energy and Surface Engineering Department of Engineering and Innovation, The Open University, Milton Keynes MK7 6AA, UK; satheesh.krishnamurthy@open.ac.uk
[5] RML Consultancy and Fabrication, Noida 201301, Uttar Pradesh, India; lalitmbharadwaj@hotmail.com
* Correspondence: nanoashish@gmail.com

Abstract: Pesticides are unavoidable in agriculture to protect crops from pests and insects. Organophosphates (OPs) are a class of pesticides that are more harmful because of the irreversible inhibition reaction with acetylcholinesterase enzyme, thereby posing serious health hazards in human beings. In the present work, a sensitive and selective immuno-sensing platform is developed using gold inter-digitized electrodes (Au-IDEs) as substrates, integrated with a microfluidic platform having the microfluidic well capacity of 10 µL. Au-IDE having digit width of 10 µm and gap length of 5 µm was used in this study. The surface morphological analysis by field-effect scanning electron microscopy (FE-SEM) and atomic force microscopy (AFM) revealed the direct information regarding the modification of Au-IDEs with anti-parathion (Anti-PT) antibodies. In SEM analysis, it was seen that the Au-IDE surface was smooth in contrast to the Anti-PT modified surface, which is supported by the AFM studies showing the surface roughness of ~2.02 nm for Au-IDE surface and ~15.86 nm for Anti-PT modified surface. Further, Fourier transform infra-red (FTIR) spectroscopic analysis confirms the immobilization of Anti-PT by the bond vibrations upon the successive modification of Au-IDE with -OH groups, amine groups after modifying with APTES, and the amide bond formation after incubation in Anti-PT antibody. Electrochemical impedance spectroscopy (EIS) was carried out for the electrochemical characterization and for testing the sensing performances of the fabricated electrode. The developed immuno-sensor provided a linear range of detection from 0.5 pg/L^{-1} µg/L, with a limit of detection (LoD) of 0.66 ng/L and sensitivity of 4.1 $M\Omega/ngL^{-1}/cm^2$. The sensor response was also examined with real samples (pomegranate juice) with good accuracy, exhibiting a shelf life of 25 days. The miniaturized sensing platform, along with its better sensing performance, has huge potential to be integrated into portable electronics, leading to suitable field applications of pesticide screening devices.

Keywords: interdigitated electrodes; organophosphates; parathion; immune-sensor; microfluidics

check for updates

Citation: Nagabooshanam, S.; Roy, S.; Wadhwa, S.; Mathur, A.; Krishnamurthy, S.; Bharadwaj, L.M. Ultra-Sensitive Immuno-Sensing Platform Based on Gold-Coated Interdigitated Electrodes for the Detection of Parathion. *Surfaces* **2022**, *5*, 165–175. https://doi.org/10.3390/surfaces5010009

Academic Editor: Mukhtar H. Ahmed

Received: 30 November 2021
Accepted: 4 February 2022
Published: 12 February 2022

Publisher's Note: MDPI stays neutral with regard to jurisdictional claims in published maps and institutional affiliations.

Copyright: © 2022 by the authors. Licensee MDPI, Basel, Switzerland. This article is an open access article distributed under the terms and conditions of the Creative Commons Attribution (CC BY) license (https://creativecommons.org/licenses/by/4.0/).

1. Introduction

Pesticides are widely used to protect crops from pests and insects. However, these pesticides leach into the food chain, soil and water bodies, creating agricultural pollutants [1]. This causes various health hazards in human beings, such as muscular dystrophy, respiratory disorders, neurological disorders, etc. [2]. Among the class of pesticides, organophosphates are more toxic because they cause irreversible inhibition with acetylcholinesterase enzyme [3]. The conventional techniques for the detection of OPs are high-performance

liquid chromatography (HPLC), liquid chromatography (LC), gas chromatography-mass spectroscopy (GC-MS), enzyme-linked immunosorbent assay (ELISA), etc. [4,5]. The aforementioned techniques are expensive, time-consuming, and require a sophisticated analytical laboratory, skilled manpower, large sample volume, and cumbersome chemical processes. Biosensors overcome the limitations of conventional techniques, providing a cost-effective and user-friendly sensing platform that requires less response time, a low sample volume without the need of skilled manpower, and an analytical laboratory.

In a biosensor, the bio-recognition element (antibody, enzyme, aptamer, microorganism, etc.) and the immobilization (physisorption, covalent and non-covalent bonding, etc.) of the same plays an important role in the overall sensing performance. Enzyme-based sensors have been extensively used for the detection of OPs but they have some limitations such as poor selectivity, sensitivity, and reproducibility. Immuno-sensors, in which antibodies are used as receptors for the specific recognition of antigens, provide better selectivity, sensitivity, low detection limits, improved shelf life and reproducibility [6,7]. Recently electrochemical immune-sensors are popular for the qualitative and quantitative detection of OPs offering low-cost sensing platforms with good sensitivity and low detection levels. Electrochemical impedance spectroscopy (EIS) is one of the most promising techniques in the class of electrochemical techniques, which involves the direct sensing of analytes based on the simple affinity complex formation [8,9]. The distinction between real and imaginary components of impedance and studying their unique behavior at various signal frequencies makes it an extremely efficient and sensitive technique for electroanalytical sensing applications [10,11]; as such, it is envisaged to effectively monitor the presence of OPs (parathion in our case).

IDEs consist of two interlocking but separated metal plates, with each having several individual digits which overlap with those of the other section, essentially creating the same structure as micro/nano-fabricated capacitors [12]. Applying a voltage to IDEs, either AC or DC, creates an electric field between the digits. This electric field can be disrupted and altered by the presence of specific target biomolecules such as cells or electrically active labels. The resulting change in current or impedance can then be calibrated to specific concentrations of the desired analyte with significant accuracy and sensitivity [13–18]. Compared to the other conventional electrodes, IDEs provide various advantages such as less sample volume, low ohmic drop, increased signal-to-noise ratio, less use of expensive antibodies or other bio-recognition elements, device miniaturization, real-time monitoring, rapid reaction kinetics, less response time and low detection limits. It is hence envisaged that the use of such interdigitated platforms could aid in rapid, efficient and sensitive immune-sensing of parathion in the food chain.

As discussed in the previous sections, the need of the hour is to fabricate a sensor which is a selective, sensitive platform which provides a rapid response time with minimal fabrication steps. In the present work, a selective immuno-sensing platform using IDE was explored for the ultra-sensitive detection of parathion. In this work, a realistic and simple immobilization methodology is adopted which avoids the conventional immobilization scheme to immobilize anti-parathion (Anti-PT) antibodies on the Au-IDE surface. The utilized Au-IDEs and the different immobilization strategy minimizes the tedious sensor fabrication procedures, thereby reducing the cost and fabrication time. The integration of the microfluidic well platform having the well capacity of 2 to 10 μL minimizes the sample volume. Anti-parathion immobilized Au-IDEs provided a better platform for the ultra-sensitive and selective detection of parathion in real fruit (pomegranate juice) samples. The selectivity and stability of the fabricated immuno-sensor were also tested. The developed sensor poses huge potential for portable-device integration and real-time field sample analysis.

2. Experimental

2.1. Materials and Instruments

Anti-parathion, parathion, chlorpyrifos, monocrotophos, malathion, bovine serum albumin, and APTES were purchased from Sigma Aldrich, (St. Louis, MO) USA. Sodium chloride (NaCl), sodium dihydrogen orthophosphate (NaH_2PO_4) and disodium hydrogen orthophosphate (Na_2HPO_4) were purchased from Fisher Scientific (Hampton, NH, USA). All experiments were performed using Milli-Q deionized water (DI water) having a resistance value of 18.2 MΩ from an ELGA water purifier, and all chemicals were analytical grade and used without further purification. All experiments were repeated thrice (n = 3), and the standard deviation is plotted for error bars using the software Origin Pro9.

The electrochemical impedance spectroscopy (EIS) was performed using potentiostat/galvanostat (Multiautolab MA204, Autolab, Utrecht, The Netherlands). Thin-film gold interdigitated electrodes (IDEs) having 10 mm height, 6 mm width, 0.75 mm thickness (digit width- 10 µm and digit gap- 5 µm) and all-in-one microfluidic platform facilitating a low reagent consumption (2 µL to 10 µL) were purchased from Micrux Technologies Ltd., Spain. Fourier transform infrared (FTIR) spectroscopic analysis was performed using Perkin Elmer Frontier ATR mode in the spectral range of 400 to 4000 cm^{-1}. The surface morphological analysis was performed using FE-SEM Tescan MIRA II (Libusina, Czech Republic), Oxford INCA Panta-FETx3. The surface roughness studies were conducted by AFM and were carried out using a Multimode IIIa Scanning Probe Micro-scope from Bruker in tapping mode with RTESP tips of radius of curvature ~10 nm.

2.2. Fabrication of Immuno-Sensor

IDEs were cleaned using acetone, ethanol DI water sequentially by sonicating for 5 min in each solution. The cleaned IDEs were dried in air at room temperature (~27 to 37 °C). Immuno-sensor was fabricated by simplified protocol which follows the reported work from Vashist S. K et al. group, with little modification [19]. The stepwise fabrication of immune-sensor is shown in Figure 1. In the first step, the IDE surface was modified by -OH groups by immersing in KOH (1% w/v) (5 µL) solution for 5 min, followed by washing with D.I. water to remove unbounded molecules on the IDE surface. In the second step, the IDE surface is modified with 1% APTES solution (5 µL) for 30 min in order to have amine (NH_2) groups on the surface of the electrode for the effective antibody immobilization, followed by washing with D.I. water to remove unbounded molecules on the IDE surface. In the third step, 1% Anti-PT solution (5 µL) introduced for 30 min incubation at 37 °C in an incubator, followed by washing the electrode with PBS pH 7 thrice to remove unbound Anti-PT on the surface. In the final step, the unspecific sites were blocked with 1% BSA (5 µL) and the electrodes were stored at 4 °C in the refrigerator for further experiments.

2.3. Preparation of Real Vegetable Samples

First, 10 g of pomegranate was crushed using mortar and pestle and 10 mL of PBS pH 7 solution was added. In the second step, the sample was centrifuged at 3000 rpm for 15 min and the supernatant was separated. Aliquots of the sample were prepared by adding a known amount of parathion to the supernatant solution, and the control sample was prepared by the same procedure explained above but without adding parathion.

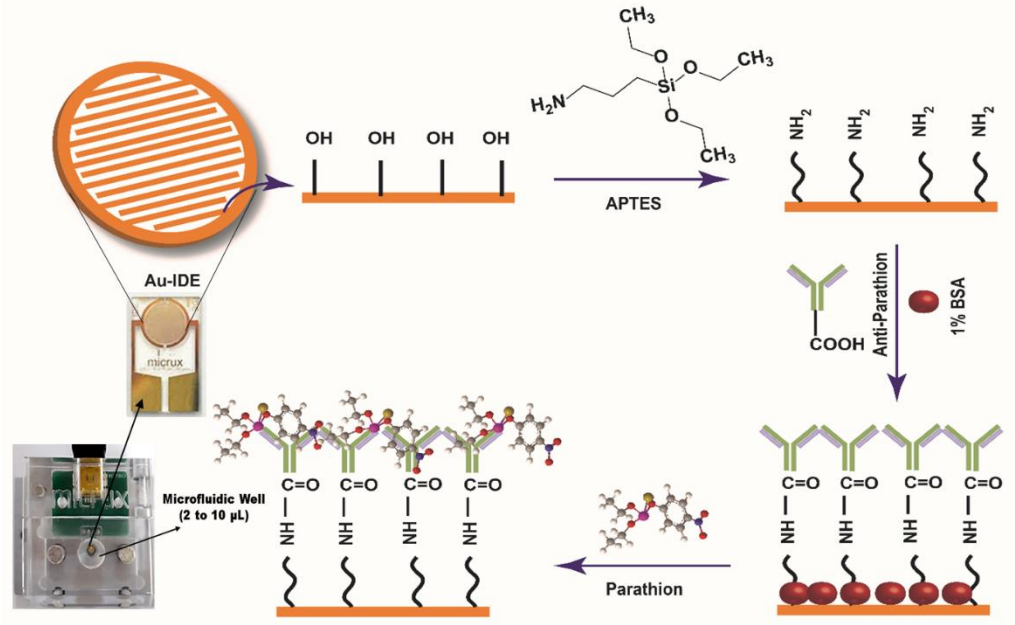


Figure 1. Schematic of stepwise fabrication of immuno-sensor (Anti-PT/Au-IDE).

3. Results and Discussion

3.1. Surface Morphology Characterization Using SEM and AFM

The surface morphological and roughness analysis by FE-SEM and AFM for the bare Au-IDE and Anti-PT/Au-IDE (antibody-immobilized Au-IDE) is shown in Figure 2. In Figure 2a, the bare Au-IDE having a finger/digit width of about 10 µm and a gap of about 5 µm is obviously realized. The uniform coating of Au on the surface of the substrate is evidenced in the inset showing FE-SEM micrograph with 1 µm scale bar.

After immobilization of antibody on the Au-IDE, the rough surface compared to the bare Au-IDE, as shown in Figure 2b, confirms the immobilization of anti-parathion onto the Au-IDE electrode. The aforementioned feature is further clarified from the three-dimensional (3D) AFM images with surface roughness assessment. The surface roughness is assessed using the Nano-Scope software by measuring the root mean square (rms) value. For Au-IDE, the roughness calculated from the rms value is ~2.02 nm with smooth and uniform Au coating as shown in Figure 2c, whereas for Anti-PT/Au-ID, higher surface roughness is observed, as shown in Figure 2d, and the roughness is calculated to be ~15.86 nm. The increase in surface roughness is due to the effective immobilization of Anti-PT biomolecules on the Au-IDE surface.

3.2. Fourier Transform Infra-Red Spectroscopic Analysis

FTIR analysis is performed at each stage of surface modification as shown in Figure 3. The bare Au-IDE surface was modified with OH groups by immersing the electrodes in KOH solution for 30 min, followed by washing in DI water. The OH modification is confirmed by the presence of broad stretching band at 3210 cm^{-1} [20]. Next, APTES is utilized to introduce amine groups on the surface of the OH modified Au-IDE surface. The peaks at 1034 cm^{-1}, 1128 cm^{-1}, 1610 cm^{-1}, 1466 cm^{-1}, 2938 cm^{-1}, 3283 cm^{-1} are attributed to Si-O-C, Si-O-Si, NH, C-N, CH_2, NH_2 groups, respectively, present in the in APTES [19,21]. The bands at 1654 cm^{-1} and 3288 cm^{-1} are attributed to the formation of amide groups after immobilizing anti-parathion [22]. The morphological analysis by the SEM and AFM is in line with the FTIR spectral data. Further electrochemical characterization is carried out to study the interfacial charge transfer parameters in the subsequent section.

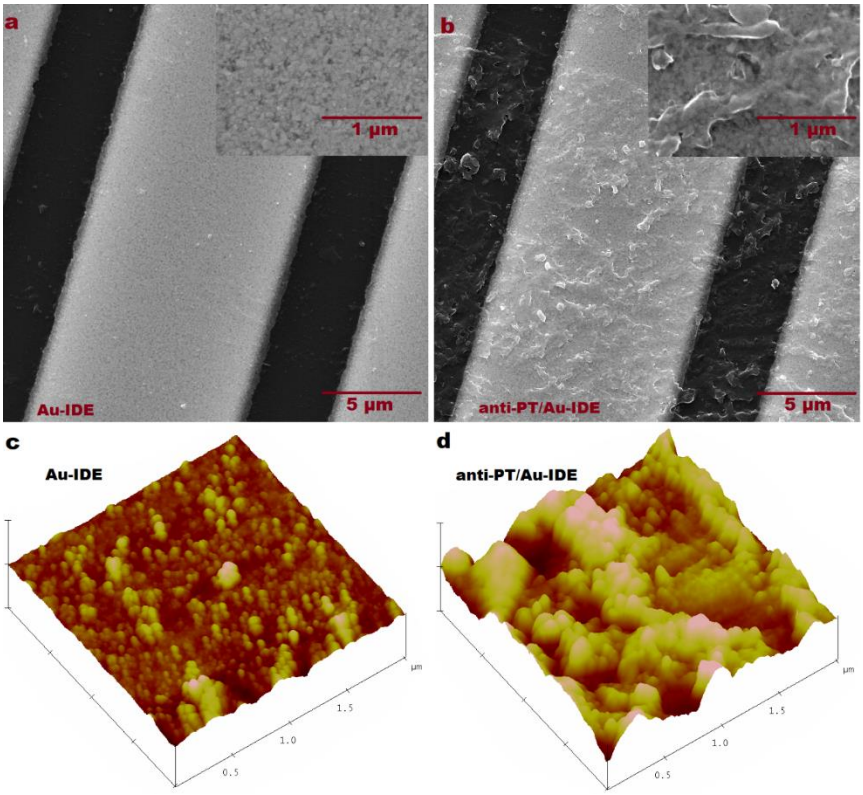


Figure 2. Surface morphological analysis of (**a**) Au-IDE and (**b**) anti-parathion/Au-IDE by SEM. Roughness analysis of (**c**) Au-IDE and (**d**) anti-parathion/Au-IDE by AFM.

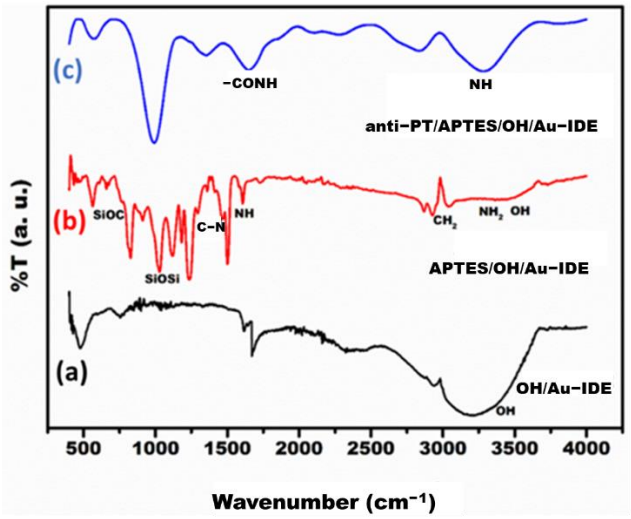


Figure 3. FTIR spectra at different stages of modification: (**a**) OH modified IDE, (**b**) after APTES modification and (**c**) after anti−parathion immobilization.

3.3. Optimization Studies

The analytical sensing performance can be varied with respect to pH and temperature. To attain better performance, the fabricated sensor is optimized for pH and temperature in the presence of 0.1 M PBS as an electrolyte. At first, different pH solutions ranging from 6 to 8 are prepared and tested on the fabricated sensor as shown in Figure 4a. It is noticed that at pH 7 the sensor showed lower charge transfer resistance (R_{ct} −40.4 MΩ); therefore, pH 7 was chosen as the optimized pH for all further experiments. A related point to consider is that at high acidic or alkali pH the immobilized antibody's stability and activity get

disrupted. The effect of temperature was also studied in the range of 15 °C to 45 °C, as shown in Figure 4b. It was observed that, at 25°C to 35 °C, the charge transfer resistance is lower compared to low (15 °C) and high (45 °C) temperatures. The possible reason could be that, at low and high temperatures, thermal inactivity or denaturation paved the way to decreased activity of immobilized antibodies; therefore, all the experiments were carried out at 25 °C.

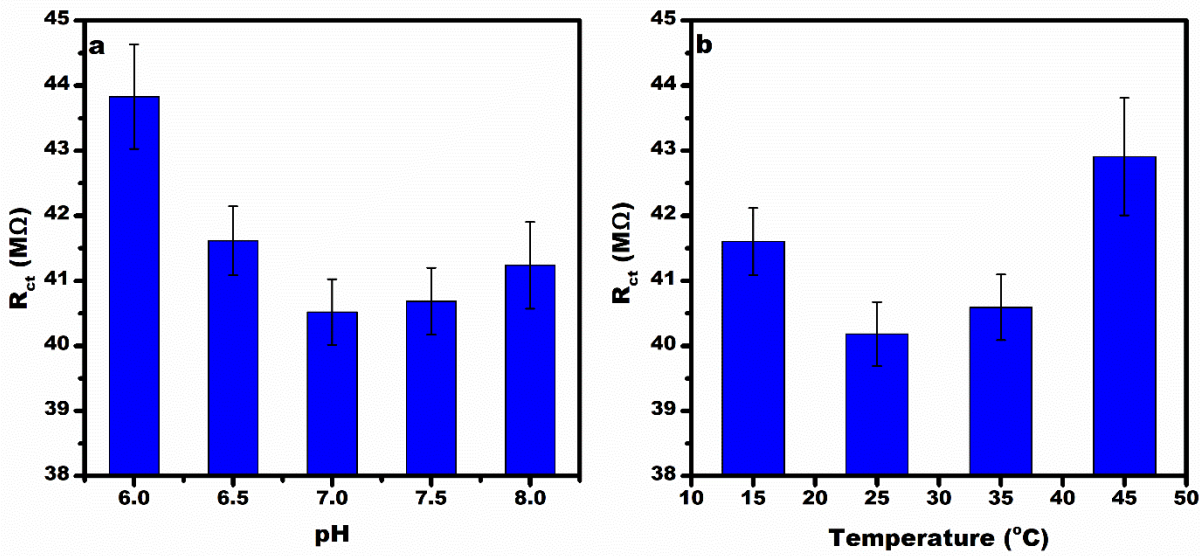


Figure 4. Effect of (**a**) pH and (**b**) temperature of anti-parathion/Au-IDE for the detection of parathion at 1 μM concentration.

3.4. Electrochemical Impedance Spectroscopic Characterization

The impedance response at various stages of surface modification of Au-IDE, which is recorded within a frequency range of 100 Hz to 50 kHz at a sinusoidal amplitude of 10 mV, is shown in Figure 5. The Nyquist spectra indicate semi-circular features corresponding to the simultaneous occurrence of charge transfer resistance (R_{ct}) and formation of double-layer capacitance near non-uniform or rough surfaces [23]. Such a non-homogeneous capacitor has been modelled using a constant phase element (CPE) and the resulting Randel's circuit is shown in Figure 5 inset.

This equivalent model has been implemented to estimate the values of various interfacial parameters (electrical elements in Randel's circuit) corresponding to electron transfer kinetics using circuit simulation. Table 1 indicates the approximate values of various interface parameters involved with electron transfer at the electrode–electrolyte interface.

Table 1. Approximate values of interfacial parameters obtained from circuit simulation using Randel's equivalent circuit.

Sl No.	Sensor Surface	R_{ct} (MΩ)	CPE (μF)
1	Au-IDE	31	1.3
2	Anti-PT/Au-IDE	47	1.2
3	PT/Anti-PT/Au-IDE	90	1.0

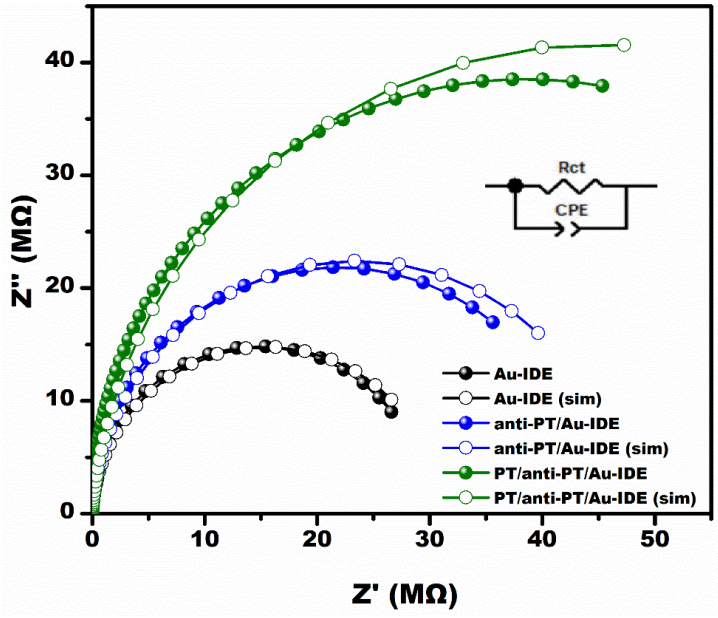


Figure 5. Impedance spectra at different surface modification stages of Au-IDE along with the Randel's equivalent circuit used to model electrode–electrolyte interfaces and curve fitting of impedance spectra by circuit simulation at different modifications of Au-IDE surfaces.

The Au-IDE surface can be observed to exhibit excellent heterogeneous electron transfer, as indicated by a low R_{ct} ~31 MΩ, which could be due to electron traversal across multiple Au electrode–electrolyte interfaces on a single IDE surface, essentially increasing the path length and hence the resistance ($R \propto l$). Meanwhile, the value of R_{ct} was found to increase to ~47 MΩ and 90 MΩ after successive surface modifications with Anti-PT and antigen–antibody complexation, respectively. The presence of Anti-PT molecules on Au effectively insulates the sensor surface which decreases the interfacial electron transfer, thereby increasing R_{ct} [24]. On the other hand, the interaction of anti-parathion with parathion leads to a typical antibody–antigen complex formation, which further passivates the sensor surface and eventually impedes the electron transfer pathway [24]. The distinct impedance response observed at each stage of sensor fabrication confirms the successful fabrication of the antibody-coated Au IDE surface for selective recognition of parathion.

3.5. Detection of Parathion by Developed Immuno-Sensor

The impedance response to various PT concentrations (0.5 pg/L to 1 μg/L) was recorded, for the Anti-PT modified Au-IDE surface, as shown in Figure 6a. The diameter of the semi-circle corresponding to R_{ct} can be observed to increase as parathion concentration is elevated to 1 μg/L. This can be attributed to the fact that at higher concentrations, a huge number of PT molecules bind to Anti-PT, thereby forming a passivating layer on the electrode surfaces, and as such, leads to an increase in sensor impedance (decrease in current) due to enhanced antibody–antigen complexation [25]. However, at low concentrations, the amount of complexation between PT and Anti-PT is comparatively less and, hence, the insulation layer thickness decreases, which results in decreased sensor impedance (or increased current). This phenomenon can then be implemented for calibrating the sensor within the specified PT concentration range. The Anti-PT/Au-IDE sensor is calibrated at 100 Hz and exhibited a linear nature within the PT concentration range of about 0.5 pg/L^{-1} μg/L (Figure 6b). A direct proportionality was established between R_{ct} and PT concentration, with line equation of log R_{ct} {MΩ} = (0.976 ± 0.031) log (PT Concentration) {ng/L} + (42.6 ± 0.0583), R^2 = 0.991. It can be observed that the R_{ct} appears to increase from ~39.2 MΩ to ~45 MΩ as the PT concentration is elevated from 0.5 pg/L to 1 μg/L, respectively, which can be well-attributed to enhanced PT–Anti-PT interactions at higher quantities, as mentioned above [25]. The LoD was calculated using the 3σ rule

(3 (Sa/b), where Sa: standard deviation of the response, and b: slope of the calibration curve) and was found to be 0.66 ng/L. The sensitivity of the developed immune-sensor was calculated by the formula Sensitivity = Slope of calibration plot ($M\Omega/ngL^{-1}$) / Active Surface Area (mm^2) and was found to be 4.1 $M\Omega/ng\ L^{-1}/cm^2$.

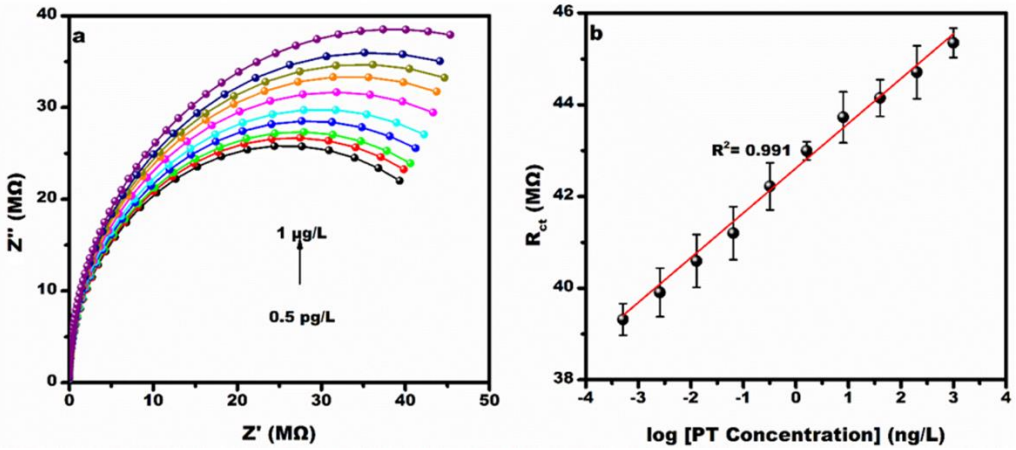


Figure 6. (**a**) Nyquist spectra and (**b**) calibration plot at different concentrations ranging from 0.5 pg/L to 1 µg/L parathion at anti-parathion/Au-IDE surfaces.

3.6. Selectivity, Stability and Real Sample Analysis

The fabricated immuno-sensor is tested for selectivity or specificity by preparing 1 µg/L solution of PT, chlorpyrifos (CPF), monocrotophos (MCP), and malathion (MT) in 0.1 M PBS as shown in Figure 7a. The R_{ct} of CPF, MCP and MT is almost equal to that of blank Anti-PT, whereas in the presence of PT, the R_{ct} was found to be increased due to the effective binding of PT to Anti-PT. The percent difference for other OPs is about ~1.8%, but with PT the difference is about ~49.8%. The specificity studies show that the fabricated immuno-sensor was more specific to parathion. The stability studies were carried out for 40 days with 5-day intervals, as shown in Figure 7b. The identical electrodes were prepared and stored at 4 °C and tested with 1 µg/L PT at 5-day intervals. It was observed that R_{ct} has remained almost similar until 25 days with a 2% decrease in R_{ct}, and it was decreased further with a 28% difference from the start day (day 0), which shows the stability of the fabricated sensor was about 25 days.

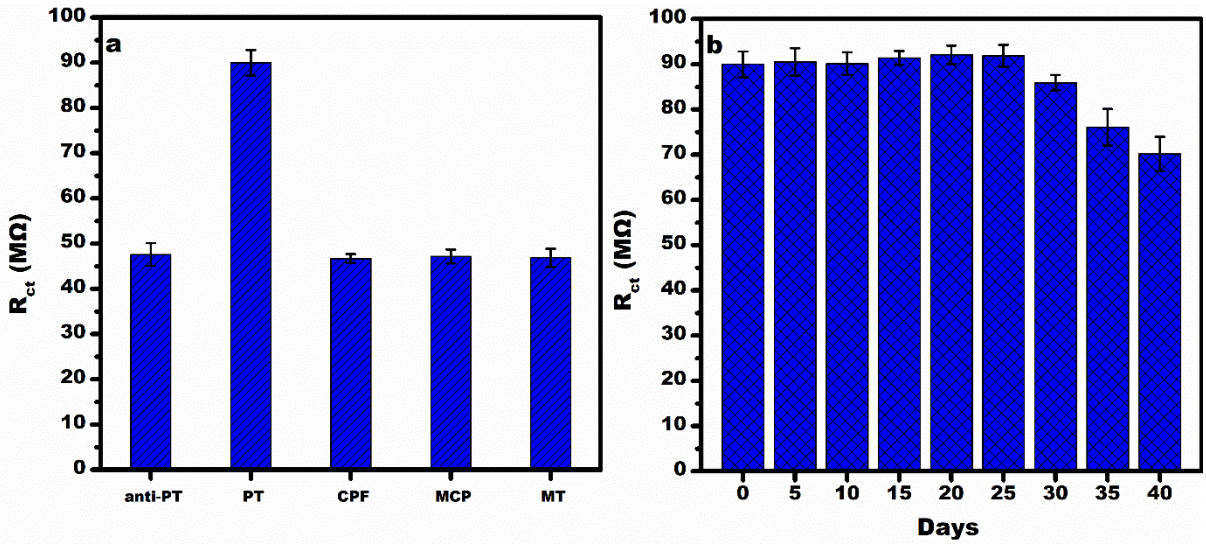


Figure 7. (**a**) Selectivity and (**b**) stability studies for anti-parathion/Au-IDE at concentration of 1 µg/L parathion.

The immuno-sensor was also tested with spiked real samples as shown in Table 2. Pomegranate juice was spiked with known concentrations of parathion and tested by the fabricated immuno-sensor. The recovery is about ~93% with RSD less than 10% showed that the developed immuno-sensor's capability for on-field sensing of OPs in the food chain. The developed sensor was compared to other reported electrochemical sensors for the detection of PT, as shown in Table 3.

Table 2. Real sample analysis of anti-parathion/Au-IDE by spiking known amount of parathion concentration in pomegranate juice.

Sample	Added (ng/L)	Found (ng/L)	% Recovery	% RSD
Pomegranate	1000	912.8	91.3	5.1
	40	37.9	94.7	7.2
	1.6	1.49	93.1	10.1
	0.0128	0.0119	92.8	9.6

Table 3. Comparison of other reported sensors for the electrochemical detection of parathion (PT).

S. No	Sensing Platform	Detection Technique	LoD (g/L)	Linear Range (g/L)	Reference
1.	[Cd(atc)(H_2O)$_2$]n/ITO (atc=2-aminoterephthalic acid)	EIS	100×10^{-9}	1 to 2×10^{-5}	[22]
2.	PANi@fMWCNT@ITO	EIS	10.2×10^{-9}	10 to 120×10^{-9}	[26]
3.	Au-Pd/rGO/CPE	SWASV	2.4×10^{-6}	2.9×10^{-6} to 0.33×10^{-2}	[27]
4.	PIL/ZIF-8/CPE	CV	2×10^{-6}	5 to 700×10^{-6}	[28]
5.	Nd-UiO-66@MWCNT nanocomposite/GCE	SWV	2.04×10^{-8}	2.9×10^{-7} to 3.5×10^{-5}	[29]
6.	Anti-PT/APTES/Au-IDE	EIS	0.66×10^{-9}	0.5×10^{-12} to 1×10^{-6}	Present work

EIS: electrochemical impedance spectroscopy, SWASV: square wave anodic stripping voltammetry, CV: cyclic voltammetry, SWV: square wave voltammetry.

4. Conclusions

A selective immuno-sensor using Au-IDE for the detection of PT is developed in this present work. The linear detection range of the sensor is found to be 0.5 pg/L to 1 µg/L, and the required sample volume is about 5 µL. The LoD was calculated to be 0.66 ± 0.01 ng/L with a sensitivity 4.1 ± 0.02 MΩ/ng L^{-1}/cm^2. The developed sensor's stability is found to be 25 days, with better selectivity towards PT compared to other OPs such as CPF, MCP and MT. The real sample analysis performed showed a good % recovery of about ~93% with RSD below 10%. Overall, the developed sensor shows a good performance, which may attribute to potential commercialization suitable for field applications. Further, the limits of detection and sensitivity can be improved by the utilization of functional nanomaterials. The extensive real sample analysis will increase the present sensor's credibility, leading to real-time detection of pesticides in various food matrices.

- ➢ Fabrication of simple Anti-PT immobilized IDE surface for electrochemical detection of PT with good selectivity and stability of about 25 days;
- ➢ The LoD for the developed sensor is 0.66 ng/L, with better sensitivity of 4.1 MΩ/ng L^{-1}/cm^2;
- ➢ The spiked pomegranate juice was tested on the developed sensor and the results show a good % recovery of about ~93% with RSD below 10%.

Author Contributions: Conceptualization, S.N., A.M., S.K. and L.M.B.; methodology, S.N. and S.R.; validation, S.N., S.R. and S.W.; formal analysis, S.N. and S.R.; investigation, S.N. and S.R.; resources, A.M. and S.K.; data curation, S.N. and S.R.; writing—original draft preparation, S.N.; writing—review and editing, S.R. and S.W.; visualization, A.M., S.K. and L.M.B.; supervision, A.M., S.W., S.K. and L.M.B.; project administration, A.M. and S.K.; funding acquisition, A.M. and S.K. All authors have read and agreed to the published version of the manuscript.

Funding: This research was funded by ICAR through NASF funded project NASF/Nano-5020/2016-17.

Institutional Review Board Statement: Not applicable.

Informed Consent Statement: Not applicable.

Data Availability Statement: The datasets used and/or analyzed during the current study are available from the corresponding author on reasonable request.

Acknowledgments: S.R., S.W. and A.M. would like to acknowledge the flagship project "Smart City" initiated by University of Petroleum and Energy Studies, Dehradun, India. This work is our initial contribution towards this project. The authors would also like to acknowledge Amity University Uttar Pradesh, Noida, India for providing access to experimental facilities.

Conflicts of Interest: The authors declare no competing interest.

References

1. Yadav, I.C.; Devi, N.L.; Syed, J.H.; Cheng, Z.; Li, J.; Zhang, G.; Jones, K.C. Current status of persistent organic pesticides residues in air, water, and soil, and their possible effect on neighboring countries: A comprehensive review of India. *Sci. Total Environ.* **2015**, *511*, 123–137. [CrossRef] [PubMed]
2. Bajgar, J. Organophosphates/nerve agent poisoning: Mechanism of action, diagnosis, prophylaxis, and treatment. *Adv. Clin. Chem.* **2004**, *38*, 151–216. [PubMed]
3. Darvesh, S.; Darvesh, K.V.; McDonald, R.S.; Mataija, D.; Walsh, R.; Mothana, S.; Lockridge, O.; Martin, E. Carbamates with differential mechanism of inhibition toward acetylcholinesterase and butyrylcholinesterase. *J. Med. Chem.* **2008**, *51*, 4200–4212. [CrossRef]
4. Stoytcheva, M.; Zlatev, R. Organophosphorus pesticides analysis. In *Pesticides in the Modern World—Trends in Pesticides Analysis*; Intech Open: Rijeka, Croatia, 2008; pp. 143–164.
5. Grimalt, S.; Dehouck, P. Review of analytical methods for the determination of pesticide residues in grapes. *J. Chromat. A* **2016**, *1433*, 1–23. [CrossRef]
6. Jiang, X.; Li, D.; Xu, X.; Ying, Y.; Li, Y.; Ye, Z.; Wang, J. Immunosensors for detection of pesticide residues. *Biosens. Bioelectron.* **2008**, *23*, 1577–1587. [CrossRef] [PubMed]
7. Shankaran, D.R.; Gobi, K.V.; Miura, N. Recent advancements in surface plasmon resonance immunosensors for detection of small molecules of biomedical, food and environmental interest. *Sens. Actuators B Chem.* **2008**, *121*, 158–177. [CrossRef]
8. Kaushik, A.; Yndart, A.; Kumar, S.; Jayant, R.D.; Vashist, A.; Brown, A.N.; Li, C.Z.; Nair, M. A sensitive electrochemical immunosensor for label-free detection of Zika-virus protein. *Sci. Rep.* **2008**, *8*, 9700. [CrossRef]
9. Cordeiro, T.A.; Gonçalves, M.V.; Franco, D.L.; Reis, A.B.; Martins, H.R.; Ferreira, L.F. Label-free electrochemical impedance immunosensor based on modified screen-printed gold electrodes for the diagnosis of canine visceral leishmaniasis. *Talanta* **2019**, *195*, 327–332. [CrossRef]
10. Lvovich, V.F. *Impedance Spectroscopy: Applications to Electrochemical and Dielectric Phenomena*; Wiley: New York, NY, USA, 2012; ISBN 978-1-118-16409-9.11.
11. Katz, E.; Willner, I. Probing biomolecular interactions at conductive and semiconductive surfaces by impedance spectroscopy: Routes to impedimetric immunosensors, DNA-sensors, and enzyme biosensors. *Electroanalysis* **2003**, *15*, 913–947. [CrossRef]
12. Parmin, N.A.; Hashim, U.; Gopinath, S.C.; Nadzirah, S.; Rejali, Z.; Afzan, A.; Uda, M.N.A.; Hong, V.C.; Rajapaksha, R.D.A.A. Voltammetric determination of human papillomavirus 16 DNA by using interdigitated electrodes modified with titanium dioxide nanoparticles. *Microchim. Acta* **2019**, *186*, 336. [CrossRef]
13. Bratov, A.; Abramova, N.; Ramón-Azcón, J.; Merlos, A.; Sánchez-Baeza, F.; Marco, M.P.; Domínguez, C. Characterisation of the interdigitated electrode array with tantalum silicide electrodes separated by insulating barriers. *Electrochem. Commun.* **2008**, *10*, 1621–1624. [CrossRef]
14. Wang, L.; Veselinovic, M.; Yang, L.; Geiss, B.J.; Dandy, D.S.; Chen, T. A sensitive DNA capacitive biosensor using interdigitated electrodes. *Biosens. Bioelectron.* **2017**, *87*, 646–653. [CrossRef] [PubMed]
15. Wang, H.; Wu, X.; Dong, P.; Wang, C.; Wang, J.; Liu, Y.; Chen, J. Electrochemical biosensor based on interdigitated electrodes for determination of thyroid stimulating hormone. *Int. J. Electrochem. Sci.* **2014**, *9*, 12.
16. Sharma, D.; Lee, J.; Seo, J.; Shin, H. Development of a sensitive electrochemical enzymatic reaction-based cholesterol biosensor using nano-sized carbon interdigitated electrodes decorated with gold nanoparticles. *Sensors* **2017**, *17*, 2128. [CrossRef]
17. Rajapaksha, R.D.A.A.; Hashim, U.; Gopinath, S.C.B.; Fernando, C.A.N. Sensitive pH detection on gold interdigitated electrodes as an electrochemical sensor. *Microsyst. Technol.* **2018**, *24*, 1965–1974. [CrossRef]
18. Bonanni, A.; Fernández-Cuesta, I.; Borrisé, X.; Pérez-Murano, F.; Alegret, S.; del Valle, M. DNA hybridization detection by electrochemical impedance spectroscopy using interdigitated gold nanoelectrodes. *Microchim. Acta* **2010**, *170*, 275–281. [CrossRef]
19. Vashist, S.K.; Schneider, E.M.; Luong, J.H.T. Surface plasmon resonance-based immunoassay for human fetuin A. *Analyst* **2014**, *139*, 2237. [CrossRef]

20. Hadjiivanov, K. Identification and characterization of surface hydroxyl groups by infrared spectroscopy. *Adv. Catal.* **2014**, *57*, 99–318.
21. Li, S.Y.; Ma, W.; Zhou, Y.; Chen, X.; Ma, M.; Xu, Y.; Ding, Z.; Wu, X. 3-aminopropyltriethoxysilanes modified porous silicon as a voltammetric sensor for determination of silver ion. *Int. J. Electrochem. Sci.* **2013**, *8*, 1802–1812.
22. Deep, A.; Bhardwaj, S.K.; Paul, A.K.; Kim, K.H.; Kumar, P. Surface assembly of nano-metal organic framework on amine functionalized indium tin oxide substrate for impedimetric sensing of parathion. *Biosens. Bioelectron.* **2015**, *65*, 226–231. [CrossRef]
23. Roy, S.; John, A.; Nagabooshanam, S.; Mishra, A.; Wadhwa, S.; Mathur, A.; Narang, J.; Singh, J.; Dilawar, N.; Davis, J. Self-aligned TiO_2-Photo reduced graphene oxide hybrid surface for smart bandage application. *Appl. Surf. Sci.* **2019**, *488*, 261–268. [CrossRef]
24. Mojsoska, B.; Larsen, S.; Olsen, D.A.; Madsen, J.S.; Brandslund, I.; Alatraktchi, F.A. Rapid SARS-CoV-2 detection using electrochemical immunosensor. *Sensors* **2021**, *21*, 390. [CrossRef]
25. Yakoh, A.; Pimpitak, U.; Rengpipat, S.; Hirankarn, N.; Chailapakul, O.; Chaiyo, S. Paper-based electrochemical biosensor for diagnosing COVID-19: Detection of SARS-CoV-2 antibodies and antigen. *Biosens. Bioelectron.* **2021**, *176*, 112912. [CrossRef] [PubMed]
26. Nagabooshanam, S.; John, A.T.; Wadhwa, S.; Mathur, A.; Krishnamurthy, S.; Bharadwaj, L.M. Electro-deposited nano-webbed structures based on polyaniline/multi walled carbon nanotubes for enzymatic detection of organophosphates. *Food Chem.* **2020**, *323*, 126784. [CrossRef]
27. Jahromi, M.N.; Tayadon, F.; Bagheri, H. A new electrochemical sensor based on an Au-Pd/reduced graphene oxide nanocomposite for determination of Parathion. *Int. J. Environ. Anal. Chem.* **2020**, *100*, 1101–1117. [CrossRef]
28. Wei, L.; Huang, X.; Zheng, L.; Wang, J.; Ya, Y.; Yan, F. Electrochemical sensor for the sensitive determination of parathion based on the synergistic effect of ZIF-8 and ionic liquid. *Ionics* **2019**, *25*, 5013–5021. [CrossRef]
29. Khoshsafar, H.; Karimian, N.; Nguyen, T.A.; Fakhri, H.; Khanmohammadi, A.; Hajian, A.; Bagheri, H. Enzymeless voltammetric sensor for simultaneous determination of parathion and paraoxon based on Nd-based metal-organic framework. *Chemosphere* **2022**, *92*, 133440. [CrossRef]